Journal of Advanced Research in Fluid Mechanics and Thermal Sciences

Journal homepage:
https://semarakilmu.com.my/journals/index.php/fluid_mechanics_thermal_sciences/index
ISSN: 2289-7879

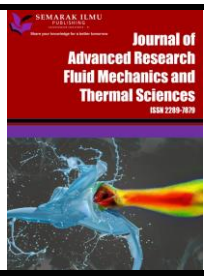

Structural Properties of Al-Li-Zn Borate Glass Activated with Dysprosium (Dy^{3+}) for Radiation Dosimeter

Efenji Godwin Irinam[1,2,*], Iskandar Shahrim Mustafa[1], Nur Nabihah Yusof[1], Rabba James Anthony[2], Munirah Jamil[1], Ferdinand Ayim Kamgba[4], Ushie Patrick Obogo[4], Umar Sa'ad Aliyu[3], Nabasu Seth Ezra[1], Thair Hussein Khazaalah[1], Hayder Salah Naeem[1], Aduragbemi Olaoluwa Oke[5]

[1] School of Physics, Universiti Sains Malaysia, 11800 USM, Penang, Malaysia
[2] Federal University Lokoja P.M.B. 1154 Kogi State, Nigeria
[3] Department of Physics, Federal University Lafia P.M.B. 146, Lafia, Nigeria
[4] Cross River University of Technology PMB 1123, Calabar, Nigeria
[5] Department of Physics, Federal University Oye-Ekiti, Nigeria

ARTICLE INFO

Article history:
Received 9 May 2024
Received in revised form 27 August 2024
Accepted 9 September 2024
Available online 30 September 2024

Keywords:
Al-Li-Zn Borate glass; structural properties; Dysprosium activation; radiation dosimeter; optical properties; Thermoluminescence (TL)

ABSTRACT

This study explores the properties of Al-Li-Zn glass doped with dysprosium ions as a potential radiation dosimeter. The glass was prepared using the novel quenching technique, and various characterisations were performed to evaluate its properties. X-ray diffraction (XRD) analysis confirmed the amorphous phases in the glass. UV-vis spectroscopy revealed a noticeable absorption peak in the visible region, characteristic of the dysprosium ions. PL spectra luminous peaks at 348 nm (yellow), 529 nm (green), and 625 nm (orange hue), which corresponded to the 4H15/2 → 6P7/2, 4F9/2 → 6H15/2, 4F9/2 → 6H15/2, and 4F9/2 → 6H13/2 transitions in 1.5 and 2.5 dysprosium ions respectively. Significant decrease in T_g from 257°C in the undoped sample to 101°C in the doped sample, T_m of the doped sample dropped from 862°C to 815°C and T_c of the doped sample dropped from 756°C to 444°C, suggesting a reduced crystallisation threshold. FTIR analysis demonstrated that OH groups displayed peaks within the 2200 to 4000 cm range. Stretching vibrations of BO3 units occurred between 1200 and 1600. Stretching vibrations of BO4 units were observed between 800 and 1200; these show that the presence of Dy^{3+} and zinc oxide altered the arrangement of the glass structure, causing a transformation from B03 groups to B04 groups. This transformation leads to defects in a stable trap environment suitable for thermoluminescence phenomena. Considering its properties and optical characteristics, the samples with 1.5 and 2.5 mol % of Dy^{3+} showed remarkable thermoluminescence properties, suggesting its suitable use as a dosimeter to gauge radiation exposure. The glass demonstrates stability and absorption capability, making it worth considering for radiation detection applications.

* *Corresponding author.*
E-mail address: godwin.efenji@fulokoja.edu.ng

https://doi.org/10.37934/arfmts.121.2.7389

1. Introduction

Due to the increasing need for precise and dependable radiation detection techniques across various industries, including environmental monitoring, industry, and medicine, developing improved materials for radiation dosimetry applications has attracted much interest recently [1]. Because of their advantageous structural and luminous characteristics, borate glasses activated with rare-earth ions have become one of the most promising materials for radiation dosimeters [2].

The primary goal of this introduction is to examine the structural characteristics of Al-Li-Zn borate glass activated by Dy^{3+} ions for use in radiation dosimetry applications, namely as thermoluminescence dosimeters (TLDs) and radiation dosimeters [3]. Borate glasses provide a flexible platform for adding dopant ions and customising their characteristics. They are renowned for their outstanding optical transparency, thermal stability, and ease of production [4,5].

Adding Dy^{3+} ions to the borate glass matrix create luminescent centres that may effectively use thermoluminescence to transform absorbed ionising radiation energy into visible light [6]. Because of this characteristic, they can be used as radiation dosimeters, which allow for precise dose measurements across a broad range of radiation energy and dosage rates because the intensity of light emitted is proportionate to the dose of absorbed radiation [7].

Optimising the dosimetric performance of these glasses requires understanding their structural properties. Their luminescence and dosimetric qualities are determined mainly by structural characteristics such as the coordination environment around the dopant ions, the existence of structural defects, and the crystalline or amorphous structure of the glass matrix [8,9]. Thus, to better understand the mechanisms underlying the radiation response of Dy^{3+} activated borate glasses, and to improve their effectiveness as radiation dosimeters, extensive research on their structural characteristics is required [10-12].

Glass structures containing zinc oxide function as an intermediate oxide, either as a network former or modulator [13,14]. Zinc ions behave like any other typical alkali oxides octahedrally coordinated when acting as a network modifier. As the former, ZnO enters the network with ZnO_4 structural units [14]. Balu *et al.,* [14] described, ZnO plays a dual role in zinc borate glasses. In their work, Balu *et al.,* [14] also emphasise how adding ZnO improved the network structure. The Zn^{2+} ions integrated into the network function as a former, according to spectroscopic investigations and the elastic characteristics of the glass compositions [14].

This work explores the possibility of the Al-Li-Zn borate glass system for thermoluminescence dosimetry by examining dysprosium's structural and optical properties and notable influence. The fabricated glass samples, when tested for radiation dosimeters, the Al-Li-Zn borate glass samples with Dy^{3+} activation show good thermoluminescence characteristics, structural stability, and radiation sensitivity. Their molar volume is 29.78 cm^3/mol, and their density is 2.675 g/cm^3, indicating significant radiation absorption. The glass exhibits substantial changes in luminescence and a well-formed matrix with thermal stability at optimal Dy^{3+} doping. Their remarkable dosimetric properties are highlighted by their low fading rate of 1% and exceptional sensitivity of 6527.9 nC/gmGy.

2. Methodology

2.1 Glass Composition and Instrumentation

Table 1 lists the precise chemical makeup and equipment utilised to create Al-Li-Zn borate glass for radiation dosimetry. High purity levels of aluminium oxide (0.1% impurity), lithium oxide (0.1% impurity), zinc oxide (0.1% impurity), boric oxide (0.2% impurity), and dysprosium oxide (0.1% impurity) are the raw materials that are all obtained from Sigma-Aldrich [15].

Table 1
Chemical composition and Instrumentation in this study with percentage impurities

S/N	Chemical name	Symbol	Impurities (%)	Manufacturer
1	Aluminium Oxide	Al_2O_3	0.1	Sigma-Aldrich
2	Lithium Oxide	Li_20	0.1	Sigma-Aldrich
3	Zinc Oxide	ZnO	0.1	Sigma-Aldrich
4	Borate Oxide	B_30_2	0.2	Sigma-Aldrich
5	Dysprosium Oxide	Dy_20_2	0.1	Sigma-Aldrich
Instrumentation				
1	Melting Furnace	-	-	Carbolite Gero
2	X-ray Diffraction (XRD) Machine	-	-	Bruker D8 Advance
3	UV-Vis Spectrophotometer	-	-	PerkinElmer Lambda 950
4	Fourier-Transform Infrared (FTIR) Spectrometer	-	-	PerkinElmer Spectrum 100
5	Thermogravimetric Analyzer (TGA)	-	-	TA Instruments Q50
6	Field Emission Scanning Electron Microscope (FESEM)	-	-	JEOL JSM-7800F
7	Fluorescence Spectrometer	-	-	PerkinElmer LS 55

Several high-precision instruments were used in the manufacturing and analytical operations. Carbolite Gero was the manufacturer of the Melting Furnace, which was essential to the glass fabrication process. Utilising a Bruker D8 Advance X-ray diffraction (XRD) machine, the structural investigation was carried out. A PerkinElmer Lambda 950 UV-Vis Spectrophotometer was used to assess the optical properties, and a PerkinElmer Spectrum 100 Fourier-Transform Infrared (FTIR) Spectrometer was used to analyse the chemical structure. A Thermogravimetric Analyzer (TGA) Q50 from TA Instruments was used to evaluate the materials' thermal stability. A JEOL JSM-7800F Field Emission Scanning Electron Microscope (FESEM) was used for morphological investigations, and a PerkinElmer LS 55 Fluorescence Spectrometer was used to analyse the photoluminescence spectra. The glass samples were precisely characterised and evaluated for possible application in radiation dosimetry thanks to this extensive set of top-of-the-line equipment [1].

2.2 Methods and Glass Fabrication

The fabrication process involved the use of the general melting quenching technique to create glass samples containing a mixture of

$(Dy_2O_3]_y–[(Li_2O)_x–(Al_2O_3)–(ZnO)_{0.02}–(B_2O_3)_{0.6-x}]_{1-y}$) in mole percent.

As shown in Table 1 and Table 2, the raw materials, including Al_2O_3 (99.9% purity), Li_2O (99.99% purity), B_2O_3 (99.8% purity), ZnO (99.9% purity), and Dy^{3+} after purchase, varying mole percentages (0, 0.5, 1.5, 2.5, 3.4, and 4.8) were pulverised. The required amounts of Al_2O_3, Li_2O, B_2O_3, ZnO and Dy^{3+} (with Dy^{3+}taking on values of 0, 0.5, 1.5, 2.5, 3.4, and 4.8 moles, respectively) were manually combined and mixed for 20 minutes using a grinding machine to obtain a fine powder. This mixture was then dissolved in a platinum crucible and placed in an electrical heating furnace, where it was heated at 1300 °C for 3 hours to ensure a homogeneous melt. Subsequently, the molten samples were annealed for 1 hour at 400°C in a stainless-steel mould. The mould and the substance were then allowed to cool to reach the ambient temperature, around 36-37°C, as seen in Figure 1 below.

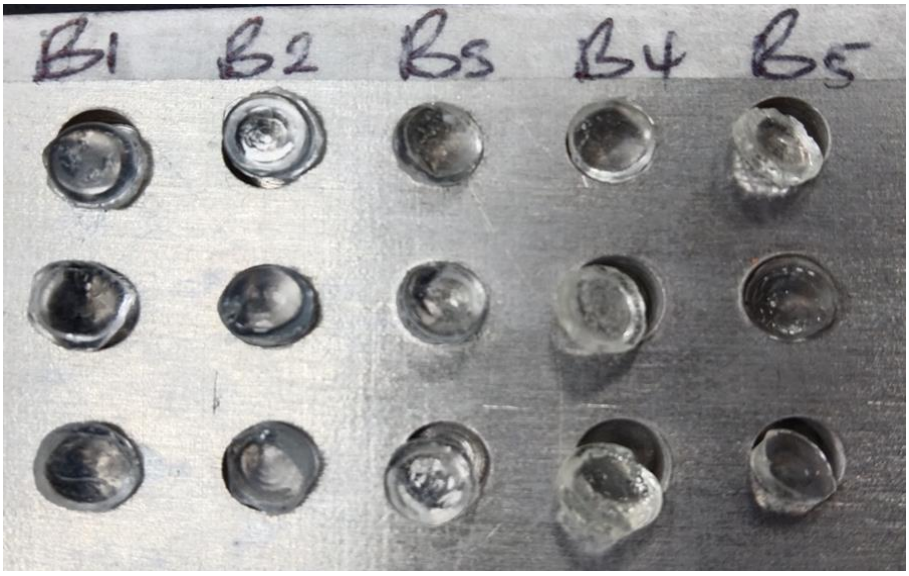

Fig. 1. Image of the fabricated Al-Li-Zn borate glass

2.3 Glass Characterisations

The infrared spectra of the glasses were measured using a Perkin Elmer infrared spectrophotometer from Japan while maintaining room temperature. We took the measurements within the wavelength range of 400 to 4000 cm^{-1}. Due to accuracy, each sample's spectrum value is repeated multiple times to minimise errors. We examined the samples' optical properties and compositions using a UV-VIS NIR imaging spectrophotometer, operating within the 100 to 600 nm wavelength range. We evaluated the glass-forming capacity and stability of the samples using a Perkin Elmer Pyris Diamond TG/DTA (6300). The instrument has a copper target and a nickel filter. The measurements were conducted at 40 kV and 30 mA, with a heat transfer rate of 10 °C per minute, covering a temperature range of 50 to 1000°C. The samples were held at 1000 °C for 10 minutes with a precision of 1°C.

3. Results and Discussion

3.1 Glass Composition

Table 2 shows the composition of Al-Li-Zn borate glass in batches (B1-B6) based on previous studies and desired qualities. The desired composition of the glass, such as Al_2O_3, Li_2O, ZnO, B_2O_3, and Dy_2O, was determined following the equation

$$(Dy_2O_3]_y–[(Li_2O)_x–(Al_2O_3)–(ZnO)_{0.02}–(B_2O_3)_{0.6-x}]_{1-y})$$

The required fractional moles of each batch were computed using the desired mole percentages and the mole weights of each chemical as suggested by the chemical equation, which guaranteed that the glass batch's stoichiometric ratios were applied correctly. The exact quantities of every raw item were determined using an analytical balance. The weights were computed based on the necessary moles and the molecular weights of the compounds. The weighted raw components were well combined to make the batch homogeneous [1,16].

Table 2
Composition of Al-Li-Zn borate glass, both with and without the addition of Dy^{3+} doping

Glass Samples	Glass Compositions (Mole Fraction %)				
	Dy_2O_3	Li_2O	Al_2O_3	ZnO	B_2O_3
B1 (CS)	0	4.013	27.385	21.857	46.745
B2	0.499	3.993	27.249	21.748	46.512
B3	1.485	3.953	26.978	21.533	46.051
B4	2.455	3.914	26.713	21.320	45.597
B5	3.411	3.876	26.451	21.112	45.151
B6	4.816	3.819	26.066	20.805	44.494

3.2 X-ray Diffraction Analysis (XRD)

X-ray diffraction (XRD) analysis is used to investigate the properties of different materials, including glasses. When studying the Al-Li-Zn doped Dy Borate glass for radiation dosimetry purposes, XRD analysis plays a significant role in understanding and identifying the crystal structure, quantifying the amounts of crystalline and non-crystalline phases, determining lattice parameters, and analysing the size of crystal particles [13,16]. These valuable insights contribute to understanding how the glasses' structure relates to its function and potential use as a radiation dosimeter. Figure 2 displays our observations. From analysis, these samples reveal no Bragg peaks in measured XRD patterns. This outcome confirms that the samples were entirely amorphous without crystalline phases [17,18].

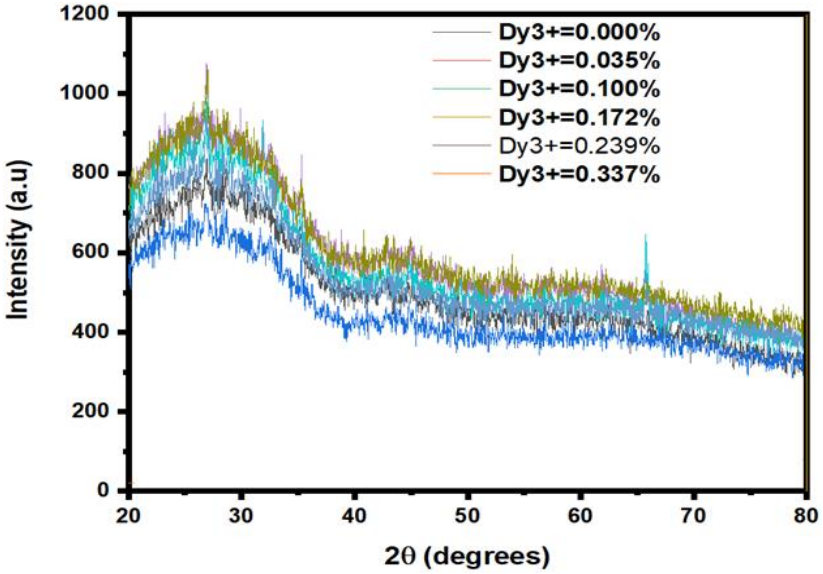

Fig. 2. The XRD spectra of undoped and Dy^{3+} doped Al-Li-Zn borate glass examined

3.3 Physical Properties

One of the essential physical properties analysed is the density of the fabricated glass. The thickness is to identify the influence of the structural rigidity and variation of the geometric configurations [19]. It was verified using Archimedes' principle, as seen in Eq. (1) with the values in Table 3.

$$\rho = \frac{a}{a-b}\rho_{dist.water} \quad (1)$$

Here, ρdist. Water is the density of the distilled water, a is the weight of the glass sample in the air, and b is the weight of the glass sample in the distilled water [10,20].

We calculated the Molar volume (Vm) using Eq. (2); the values are in Table 3.

$$V_m = \frac{M_{wt}}{\rho} \tag{2}$$

Table 3
Glass Compositions, density, and molar volume of the samples

Glass Samples	Glass compositions (mole fraction %)					Density (g/cm^3) ± 0.03	Molar volume (cm^3/mol.) ± 0.03
	Dy_2O_3	Li_2O	Al_2O_3	ZnO	B_2O_3		
B1 (CS)	0	4.013	27.385	21.857	46.745	2.606	29.48
B2	0.499	3.993	27.249	21.748	46.512	2.592	29.75
B3	1.485	3.953	26.978	21.533	46.051	2.675	29.78
B4	2.455	3.914	26.713	21.320	45.597	2.695	29.79
B5	3.411	3.876	26.451	21.112	45.151	2.745	29.83
B6	4.816	3.819	26.066	20.805	44.494	2.804	29.89

In Figure 3, glass density, along with its composition and structure, is correlated, showing the molar volume, density, and fractional moles of Dy^{3+}. Since external network ions increase the number of existing atoms without appreciably altering the size of the network, the density generally also rises with the addition of these ions [21]. In this instance, the rise in density caused by the external network ions is more significant than the loss in density brought on by the network's fracture, expansion, and increase in volume [22]. Table 3 provides a summary of the glasses' densities and molar volumes.

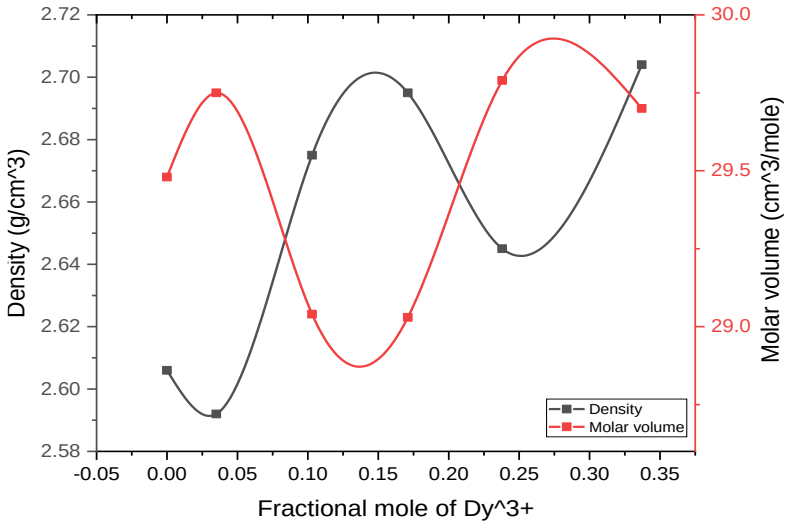

Fig. 3. Graph of density and molar volume against fractional mole of Al-Li-Zn borate glass with undoped and doped Dy^{3+}

Glass samples B3, B4, B5, and B6 in this composition have increased densities as the dopant element increases (Dy_2O_3). The changes are because the dopant's relative atomic mass is 373 times greater than the relative atomic mass of the glass former (B_2O_3), which is 70.0034. As a result, the introduction of heavy atoms into the glass system caused a comparable indirect rise in the glass density. The B2 glass sample has a lower density because the relative mass of the glass former is less than the dopant element's mass, making the glass network more compatible [23,24].

In their study, Saidu *et al.,* [25] demonstrated a relationship between the atomic radius, the value of the molar volume, and the compaction of the glass network. In other words, they clarify that the

molar volume decreases with increasing glass structure compactness [21]. As the dopant element for B2 increased, a tiny increase in molar volume was noticed in B2, demonstrating that the glass network did not constrict because of the addition of secondary flux (ZnO) [26,27].

The fact that B3, B4, and B6 have allowable molar volumes relative to B1 shows that B_2O_3 is involved in the glass network structure as a glassmaker with B04 in the glass, making the glass denser and lowering the molar volume [23,28]. Glass samples B3 and B4 have the smallest molar volumes, showing that they have the densest glass networks when compared to the other glasses [15,29].

3.4 Energy Bandgap

Analysing the material's optical absorption spectra makes it possible to learn more about the energy band gap and band structure of amorphous materials. The phenomenon involves the absorption of photons with energies more significant than the material's bandgap so that absorption spectra at lower energies give information about atomic vibration. In comparison, those at higher powers discuss the material's electronic state at the nuclear level [2]. The optical absorption spectrum is crucial for examining photon transitions that cross band gaps. The sharpest edge of the energy gap for crystal lattice is defined using the 1976 Mott and Davis formula, Eq. (3)

$$E_g = \frac{hc}{\lambda} \tag{3}$$

E_g stands for energy gap, h for Plank's constant, c for light speed, and wavelength. We are using Eq. (4) to determine the absorption edge and geometry of the band gap for an amorphous lattice [2].

$$\alpha = (hv - E_g)^n \frac{A}{hv} \tag{4}$$

where n is a constant that varies with state (n = 2 for allowed direct transitions and 1/2 for allowed indirect transitions), is the absorption coefficient, and A is a parameter that affects band tailing.

The energy band gap of all samples in Table 4 demonstrates a progressive rise and fall with the addition of modifiers and other compositions, as seen in Figure 4(a) to Figure 4(f). The direct energy bandgap, measured in eV for each produced glass sample, is plotted in Figure 4 as (αhv)2 versus E. As the composition concentration rises from 10 to 30 % with a dopant (Dy^{3+}) In sample 2, the energy bandgap increases from 3.3 to 3.9 eV [25]. Additionally, samples 3, 4, and 5 significantly decline as composition concentration rises from 30 to 80 % compared to sample 2. As the component concentration rises to 100%, sample 6 (B6) exhibits a considerable increase in the direct energy bandgap from 3.90 to 5.5 eV compared to B2. All the samples of the manufactured glass' indirect energy band gap, measured in eV, are shown in a similar graph of (hv)1/2 vs E in Figure 5. Like this, the addition of dopant and increment of other compositions causes the energy band gap for batches 2, 3, 4, and 5 to expand from 1.5 to 2.6 eV when compared with B1, which is undoped. Similarly, sample 6 reduces to 1.4 eV in the indirect bandgap energy [1,30].

Table 4
Direct energy band gap (eV) and indirect energy bandgap (eV) of the studied composition

S/N	Glass samples	Direct energy band gap (eV)	Indirect energy band gap (eV)
1	B1, undoped	3.3	2.6
2	B2	3.9	2.5
3	B3	3.5	2.0
4	B4	3.7	1.7
5	B5	3.5	1.5
6	B6	5.5	1.4

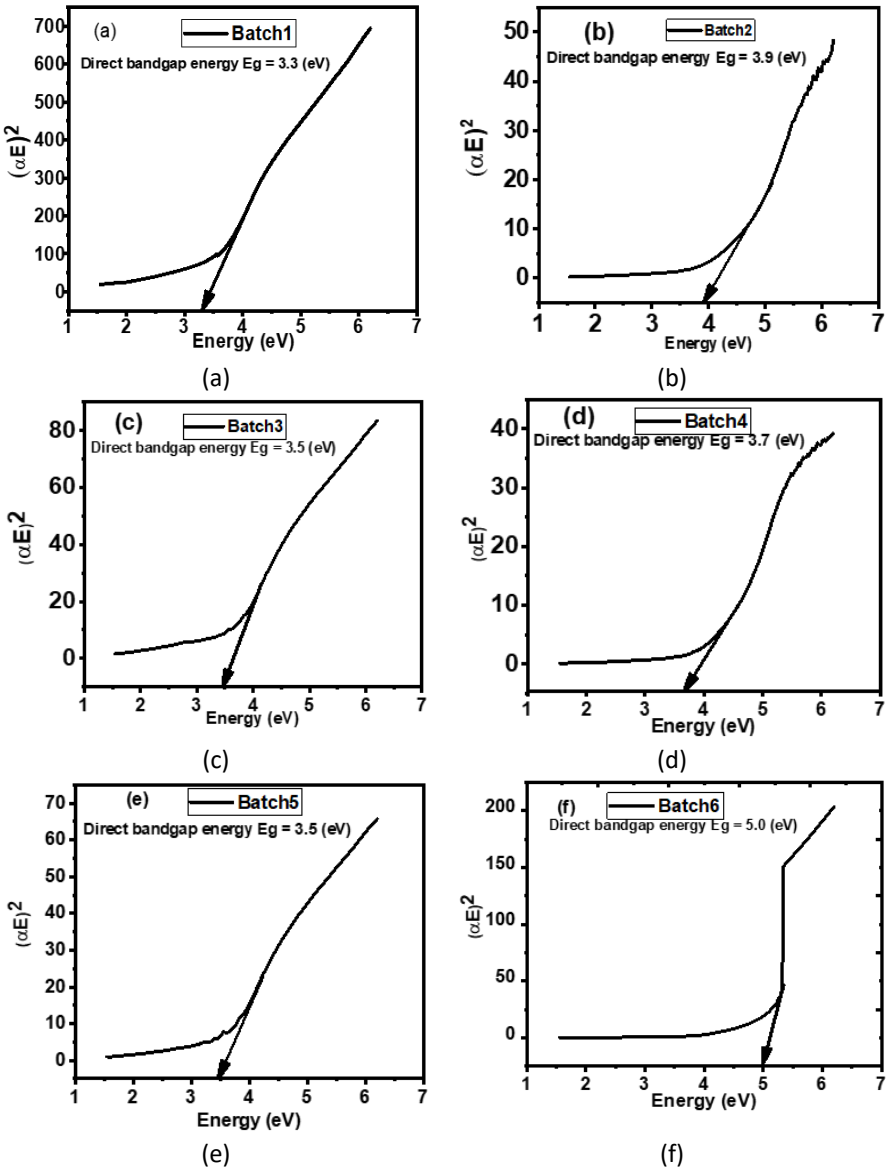

Fig. 4. Graph of direct energy bandgap of Al-Li-Zn at (a) (undoped) E_g=3.3(eV), (b) E_g=3.9(eV), (c) E_g=3.5(eV), (d) E_g=3.7(eV), (e) E_g=3.5(eV), (f) E_g=5.0 (eV)

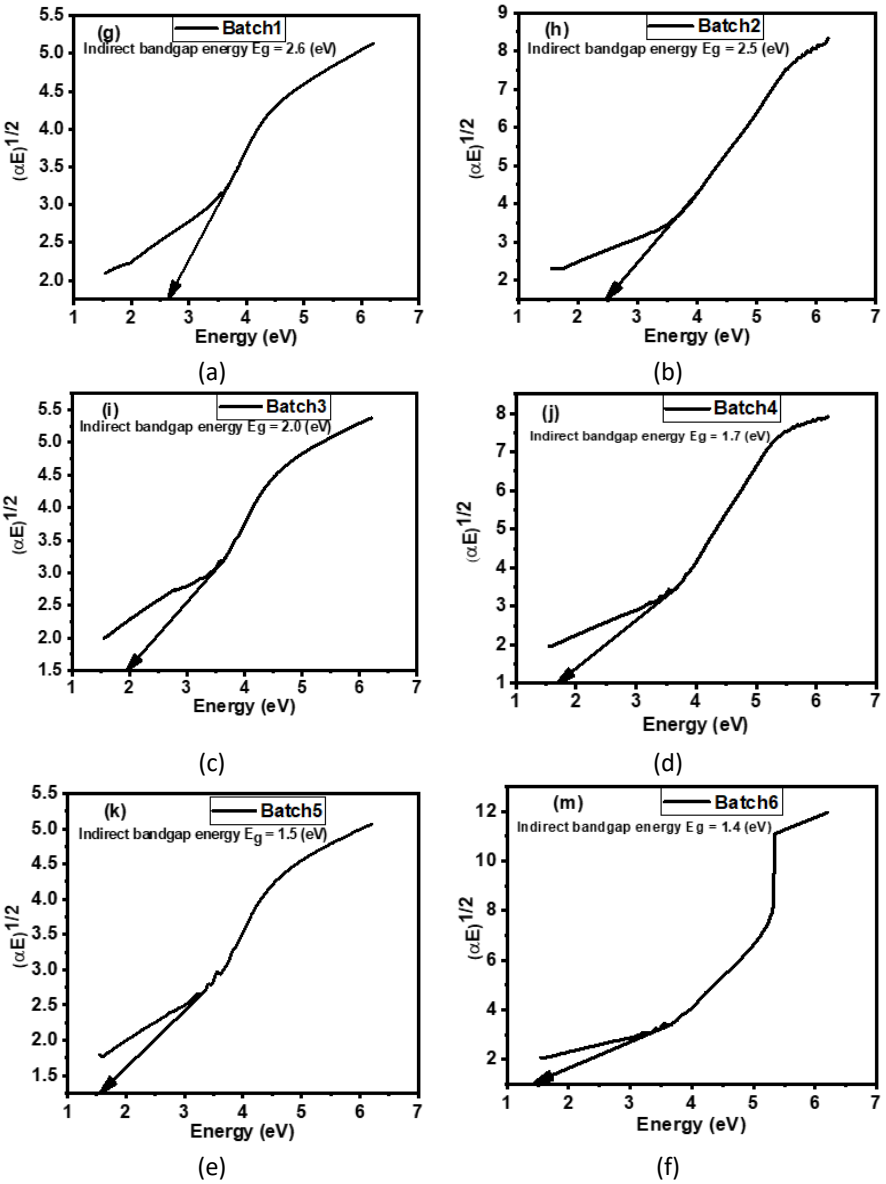

Fig. 5. Graph of indirect energy bandgap of Al-Li-Zn at (a) (undoped) E_g=2.6(eV), (b) E_g=2.5(eV), (c) E_g=2.0(eV), (d) E_g=1.7(eV), (e) E_g=1.5(eV), (f) E_g=1.4(eV)

As seen in Table 4, B1 samples have a direct bandgap energy of 3.3 eV. This relatively low direct bandgap energy makes it suitable for applications such as photovoltaic and light-emitting diodes (LEDs) that operate in the near-infrared range. B2 also has a natural bandgap energy of 3.9 eV. The higher direct bandgap energy means the materials with this energy are better at absorbing and emitting light in the ultraviolet range. Also, the B2 shows that the materials influence aluminium oxide and zinc oxide (ZnO). B3, B4, and B5 also have 3.5 eV and 3.7 eV direct bandgap energy values. These show that they are intermediate natural bandgap energies, which make them suitable for applications such as operating in the visible range of the electromagnetic spectrum. B6 has a bandgap energy of 5.5 eV. The high direct bandgap energy means that the materials are better at absorbing and emitting light in the deep ultraviolet range and, as such, are suitable for thermoluminescence [21,30].

In a transition, an indirect bandgap material requires an additional mechanism, such as phonon assistance, to conserve momentum. This different mechanism reduces the efficiency of electron-hole

recombination, and therefore, indirect bandgap materials typically have lower thermoluminescence yields than direct bandgap materials [23,31].

The indirect bandgap energy values for the concentration of Dy^{3+} (0.0, 0.5, 1.5, 2.5, 3.4, and 4.8 mol.) are 2.6, 2.5, 2.0, 1.7, 1.5, and 1.4 eV, respectively, as seen in Table 4, is the energy required for electron transitions in specific materials. Figure 6(a) to Figure 6(f) also show the graph of indirect bandgap energies with a gradual reduction of the indirect bandgap energies by introducing the Dy^{3+} dopant element. Indirect bandgap materials typically have higher energy requirements than direct bandgap materials, and therefore, their thermoluminescence properties are generally less favourable for dosimetry purposes. In thermoluminescence dosimetry, indirect bandgap materials are typically combined with direct bandgap materials to improve the detection range and accuracy. The choice of materials depends on the specific application and the desired detection range [26,31].

3.5 Fourier Transform Infrared Spectroscopy

FTIR spectroscopy (Perkin Elmer, U.S.A.) was used to analyse and confirm the bonding of the functional groups in the glass, as shown in Figure 6. In the thin pellet approach, the FTIR spectra are between 400 and 4000 cm^{-1} with a resolution of 0.85 cm^{-1} at a pressure of 77.2 MP. Each IR spectra represents the average of the standard pellets to maximise analytical errors. As shown in Figure 6, the infrared transmittance spectra of the glasses had significant, medium, weak, and broad peaks in the 400–4000 cm^{-1} area with the four sections of the borate, as shown below [31].

(i) 600 to 800 cm^{-1} for B–O–B vibrations
(ii) 800 to 1200 cm^{-1} for clusters of BO4
(iii) 1200 to 1600 cm^{-1} for BO3 groups
(iv) 2.300 to 4.000 cm^{-1} for OH groups

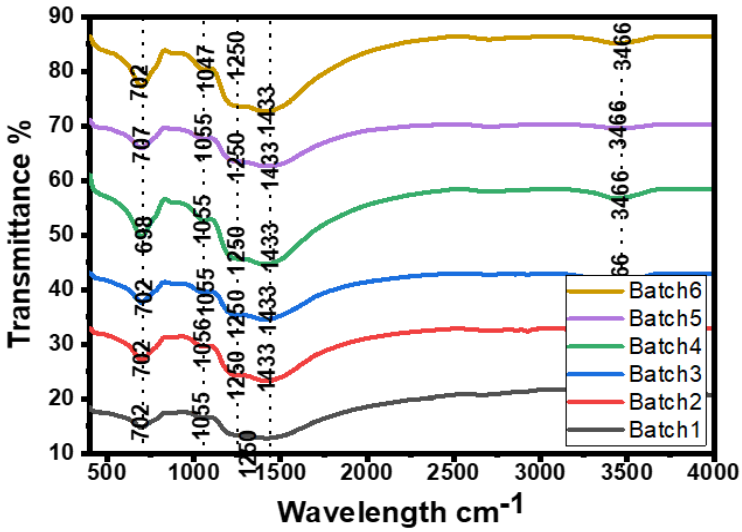

Fig. 6. FTIR spectra of Al-Li-Zn borate glass doped and undoped Dy^{3+} of various composition

According to Figure 6, the B-O-B bending vibration of BO3 and [BO4] has a band centred at 702 cm^{-1} [32]. Due to the [AlO_6] group of aluminium being present in the glass network, the intensity of the first band increases as aluminium content increases [33,34]. The FTIR study also reveals that B6's glass composition has a band of 1047 cm^{-1}, which results from the [BO4] groups' B-O-B stretching. In B5, B4, B3, B2, and B1, the band of this batch gradually shifts toward the higher wave numbers from

1047 to 1055 cm^{-1} side with an increase in the components of the glass network (Al_2O_3, B_2O_3, ZnO, LiO, and Dy^{3+}) [30,35].

Additionally, as the tetrahedra [BO4] groups in the borate network increase, the intensity of batches rises as the glass network elements increase progressively. Due to the existence of [AlO_6] units of aluminium and the effects of the secondary flux, the band bond marginally rises as the concentration of aluminium oxide and zinc oxide increases (zinc oxide). In plain terms, the presence of aluminium can be due to the coexistence of the tetrahedral [BO4] groups of borates and the aluminium [AlO_6] group [3]. The B-O stretching of [BO3] groups in the ortho and metaborate units in the network causes the band in the range of 1200 to 1600 cm^{-1}. Additionally, the energy band at 698 cm^{-1} is related to the vibration of Li+ cations against their network former, while the vibration modes found at 702 cm^{-1} are owing to the binding way of ZnO vibrations. The presence of hydrogen bonding in the OH groups is what causes the additional stretching of the bond from 3000 to 3466 cm^{-1} [36,37].

According to FTIR measurements, the concentration of the dopant and other glass network ingredients increased the stiffness and decreased the disorder of the glass. Figure 6 displays the glasses' spectral bands [32].

3.6 Differential Thermal Analysis (DTA)

The transition temperature (T_g) and crystallisation temperature (T_c) value, the glass-forming ability (GFA), and the stability of its glass network. Materials with a high T_g and a lowT_c, generally have a higher GFA and strength. In contrast, materials with a low T_g and a high T_c, have a lower glass-forming ability (GFA) and stability.

We calculated the glass forming ability (GFA.) and glass stability of the materials using Eq. (4) and Eq. (5), respectively, and the values in the Table 6.

$$\text{GFA} = (T_c - T_g) / (T_m - T_g) \quad (5)$$

$$\text{GS} = (T_c - T_g) / T_g \quad (6)$$

Table 5 provides values for three parameters, T_g, T_c, and T_m, for six batches. T_g represents the glass transition temperature, T_c indicates the crystallisation temperature and T_m represents the material's melting temperature. These parameters play a role in thermoluminescence studies as they can impact the luminescence properties of the material. For instance, T_g shows how much energy is needed to activate the luminescent centres in the material. Similarly, T_c influences how defects that generate the luminescence signal move during heating [37]. Ideally, we want a value for T_g to ensure the thermal stability of the material and a low enough value for T_c to enable efficient movement of defects during heating. Depending on what we are studying T_m might also be relevant [29].

Table 5
The parameter values of T_g, T_c and T^m of Al-Li-Zn borate glass doped Dy^{3+} at various composition

Parameters	B1	B2	B3	B4	B5	B6
T_g	257.87	411.76	448.82	454.17	0.00	423.62
T_c	754.22	768.81	663.93	758.09	0.00	771.32
T_m	862.97	827.18	813.95	845.65	0.00	856.36

Figure 7 to Figure 12 show the thermal analysis of the various glass batches. We observed that the batch 5 sample (labelled as B5) had results that significantly deviated from the expected limit or

had no results in their Differential Thermal Analysis (DTA) curve. Compared to all other manufactured samples, samples B1, B2, B3, B4, and B6 are glass former with favourable thermal stability [35].

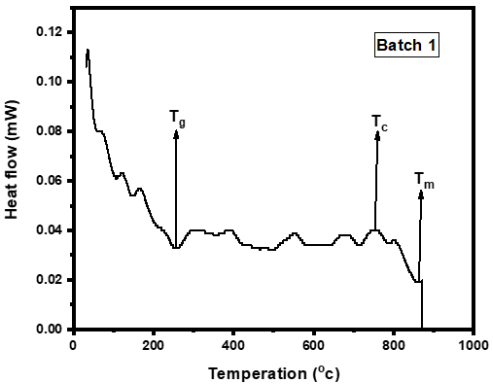

Fig. 7. Differential thermal analysis of B1 (CS) sample with Al-Li-Zn borate glass undoped Dy^{3+}

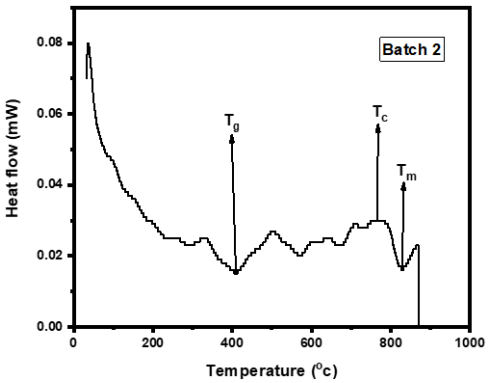

Fig. 8. Differential thermal analysis of B2 sample with Al-Li-Zn borate glass doped with 0.5 mol. of Dy^{3+}

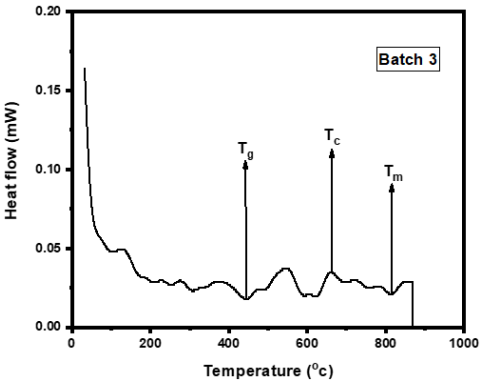

Fig. 9. Differential thermal analysis of B3 sample with Al-Li-Zn borate glass doped with 1.5 mol. of Dy^{3+}

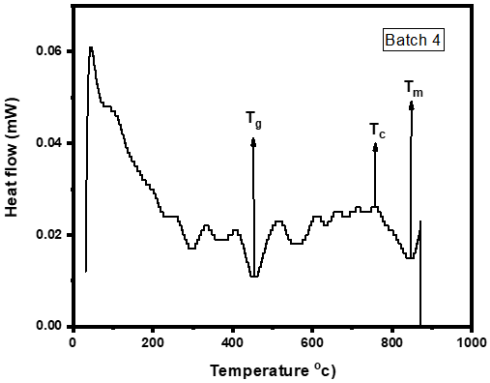

Fig. 10. Differential thermal analysis of B4 sample with Al-Li-Zn borate glass doped with 2.5 mol. of Dy^{3+}

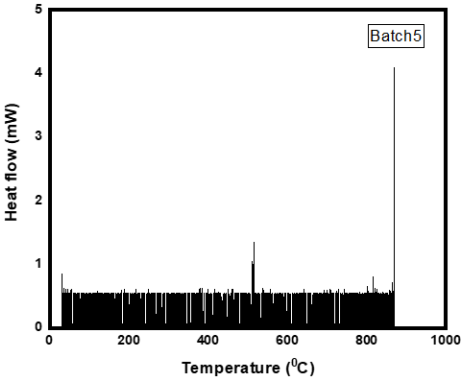

Fig. 11. Differential thermal analysis of B6 sample with Al-Li-Zn borate glass doped with 3.4 mol. Of Dy^{3+}

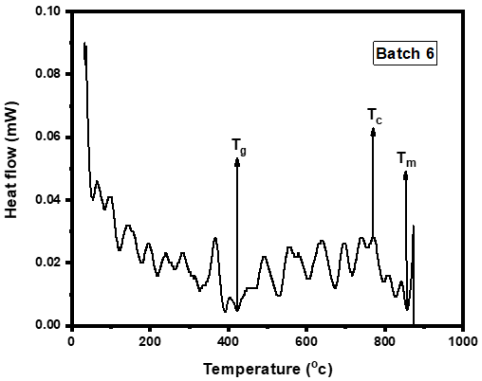

Fig. 12. Differential thermal analysis of B6 sample with Al-Li-Zn borate glass doped with 4.8 mol. of Dy^{3+}

In radiation dosimetry, finding a glass material that can maintain its glassy structure and exhibit thermoluminescence properties is essential. The ability to form a glassy structure (GFA.) and glass stability (GS) play a role in determining the suitability of a material for dosimetry applications. According to Table 6, the Al-Li-Zn borate glass doped with Dy compositions shows high values for

both GFA and GS, indicating its strong tendency to remain in a glassy state and resist crystallisation [9]. Previous study suggests that materials with glass-forming ability (GFA.) tend to have T_c/T_g ratios indicating good glass-forming capability [38]. When the GFA exceeds 0.5, it signifies stability, implying resistance against devitrification, allowing the material to remain in its glassy state across temperatures [5].

Table 6
GFA. and GS values of Al-Li-Zn borate glass doped Dy^{3+} At various composition

Measurement	B1	B2	B3	B4	B5	B6
GFA	0.82	0.86	0.59	0.78	-	0.80
GS	1.92	0.87	0.48	0.67	-	0.82

Observing Figure 7 and Figure 10, it is evident that samples B1 and B4 possess GFA values, suggesting their likelihood of containing defects or impurities of emitting light when heated. Furthermore, B1 exhibits a GS Value compared to B4, suggesting that the former sample emits light when heated, possibly indicating a higher concentration of impurities or defects. In Figure 9, B3 has a higher GFA value than B1, B2, B4, and B5, implying that this sample contains defects or impurities capable of emitting more light. Figure 7 and Figure 11 demonstrate that batches B1 and B5 have GFA Values compared to B1, B2, and B4, indicating a concentration of defects or impurities. However, the high GS value of B2 implies that this sample emits more light during the heating process than the other batches, potentially indicating a higher concentration of impurities or defects [6,30].

3.7 Photoluminescence (PL) Spectrum

A photoluminescence spectrum often exhibits bands or peaks of light emission at wavelengths, which indicate variations in the material's electrical energy levels. A photoluminescence spectrum often exhibits bands or peaks of light emission at wavelengths, which indicate variations in the material's electrical energy level [38]. When triggered by light, the locations and intensities of these peaks provide crucial information about the material's composition, behaviour, and structure. The mechanism mentioned below explains the phenomenon of PL emission in these glasses. Upon stimulation, the electrons are confined in the electron centres, essentially the host boron ions. The relaxation process subsequently releases the electrons, which Dy^{3+} ions then absorb [1]. PL is released when the holes in the boron oxygen eventually take up the electrons. PL spectra of the suggested Dy^{3+} doped Al-Li-Zn borate glass at 400 nm excitation is shown in Figure 13. Bright peaks at 348 nm (yellow), 529 nm (green), and 625 nm (orange hue) in the composition demonstrated good and unique light sensitivity; these corresponded to the 4H15/2 → 6P7/2, 4F9/2 → 6H15/2, 4F9/2 → 6H15/2, and 4F9/2 → 6H13/2 transitions in Dy^{3+}, respectively [6]. Additionally, this transition is correlated with the 4H15/2 → 6P7/2 transition in Dy^{3+} ions at 348 nm (white light), commonly employed because of its high photoluminescence (PL) efficiency as a calibration reference in radiation dosimetry. The microscopic structure of Dy^{3+} can have a significant impact on the emission channels of the doped material, particularly on the transition with selection rules of $\Delta L = \pm 2$; $\Delta J = \pm 2$ [4,5].

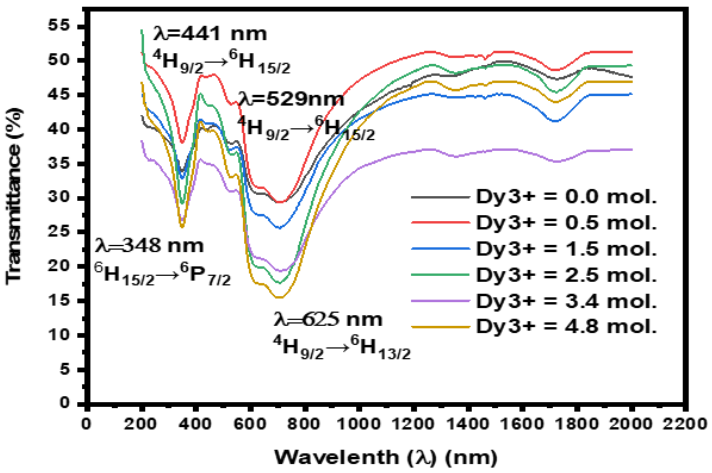

Fig. 13. Photoluminescence spectra of undoped and Dy^{3+} doped Al-Li-Zn Borate glass sample irradiated with 100 mCi gamma radiation dose

4. Conclusions

We conducted an investigation into the properties of Al-Li-Zn borate glass activated with Dy^{3+} within the composition; $[Dy_2O_3]y - [(Li_2O)x - (Al_2O_3)0.2 - (ZnO)0.02 - (B_2O_3)0.6 - x]1 - y$ for its use as a radiation dosimeter. The XRD analysis results confirmed the amorphous phase in the glass material. Additionally, the UV-Vis spectra displayed an absorption peak within the region, confirming activation by Dy^{3+} ions. The thermal stability of the glass was found to be satisfactory based on the results from TGA and DTA, suggesting its suitability for dosimetry purposes. The presence of borate and metal-oxygen bonds in the glass network was confirmed by identifying modes, while OH groups exhibited peaks within 2200 to 4000 cm^{-1} range. The stretching vibrations of BO3 units were observed between 1200 to 1600 cm^{-1}. At the same time, BO4 units showed stretching vibrations between 800 and 1200. Additionally, bending vibrations of borate segments were detected within the range of 400 to 800 cm^{-1}. Incorporating Dy^{3+} ions successfully altered the glasses' properties, resulting in radiation-sensing capabilities. The absorption peak in the region and specific vibrational modes associated with the glass network indicate the integration of Dy^{3+} ions into the glass matrix. Moreover, good thermal stability was observed in this glass, ensuring its applicability. The study reveals that samples B2 and B3, with Dy^{3+} concentrations of 1.5 moles and 2.5 moles showed remarkable thermoluminescence properties. The glass's ability to form shapes and stability has shown promise. Studying the relationship between dose and response and the glass's stability under different radiation conditions is beneficial. Overall, this research provides insights into the properties of Al-Li-Zn borate glass activated with Dy^{3+} and its potential as a radiation dosimeter, contributing to advancements in radiation detection and measurement technology. The Dy^{3+} activated Al-Li-Zn borate glass samples show good signal loss (1% over months), high sensitivity (6527.9 nC/gmGy), repeatability (7.1), and structural stability. These characteristics indicate their applicability as possible radiation dosimeters, which include strong luminous response and effective radiation absorption.

Acknowledgement
We want to express our gratitude to Universiti Sains Malaysia (USM) for providing us with research facilities and financial support through the Bridging Grant (project code BG0316; project reference 2019/0530 (304/PFIZIK/6316531)). We would also like to acknowledge the sponsorship and financial

assistance from Federal University Lokoja, Nigeria. Special thanks go out to Assoc. Professor Dr. Iskandar Shahrim Mustafa, for initiating this research and serving as our supervisor.

Conflict of interest

We declare that we have no competing interests. To maintain objectivity, our research is limited to studying glass composition for radiation dosimetry. The objectivity of our research is unaffected by any associations or connections.

Ethics approval

The research is unrelated to any ethical concern; hence, no ethical approval is needed.
Data availability Statement.
Data will be made available on request.Top of FormBottom of Form.

References

[1] White, Andrew J., Sean P. Jollota, Cliff G. Hammer, Ahtesham U. Khan, Larry A. DeWerd, and Wesley S. Culberson. "Thermoluminescent dosimeters (TLD-100) for absorbed dose measurements in alpha-emitting radionuclides." *Applied Radiation and Isotopes* 208 (2024): 111307. https://doi.org/10.1016/j.apradiso.2024.111307

[2] Bendary, A. A., Hosam M. Gomaa, A. M. Moneep, M. R. Atta, A. S. Abdel-Moety, Ali M. Ibrahim, and M. I. Sayyed. "Effect of replacing B_2O_3 with Dy_2O_3 on the structural, physical, and radiation shielding properties of sodium boroaluminate glass." *Journal of the Australian Ceramic Society* 60, no. 2 (2024): 455-469. https://doi.org/10.1007/s41779-023-00970-z

[3] Saidu, A., H. Wagiran, M. A. Saeed, H. K. Obayes, A. Bala, and F. Usman. "Thermoluminescence response of rare earth activated zinc lithium borate glass." *Radiation Physics and Chemistry* 144 (2018): 413-418. https://doi.org/10.1016/j.radphyschem.2017.10.004

[4] Yılmaz, Demet, and Tuba Akkuş. "An experimental work on radiation scattering features of some thermoluminescent dosimetry materials." *Radiation Physics and Chemistry* 216 (2024): 111456. https://doi.org/10.1016/j.radphyschem.2023.111456

[5] Ullah, Bait, Muhammad Basim Kakakhel, Shakeel Ur Rehman, Muhammad Tariq Siddique, Muhammad Munir, Khalil Ahmad, Muhammad Masood Mahmood, Mirza Wazir-ud-Din, and Iftikhar Anjum. "Synthesis and dosimetric characterization of lithium tetraborate ($Li_2B_4O_7$: Cu, Ag) thermoluminescent dosimeter with improved reproducibility and reusability." *Radiation Physics and Chemistry* 220 (2024): 111704. https://doi.org/10.1016/j.radphyschem.2024.111704

[6] Efenji, Godwin Irinam, E. K. Egeonu, I. Isah, S. F. Onimisi, F. O. Uloko, J. A. Nakale, K. J. Ayua, and M. O. Idris. "Determination of Activity Concentration of Radioactive Elements in Borehole and Well Water Samples from Adankolo New Layout Lokoja." *FUDMA Journal of Sciences* 6, no. 3 (2022): 160-166. https://doi.org/10.33003/fjs-2022-0603-950

[7] Sundararaman, Siddharth, Liping Huang, Simona Ispas, and Walter Kob. "New interaction potentials for borate glasses with mixed network formers." *The Journal of Chemical Physics* 152, no. 10 (2020). https://doi.org/10.1063/1.5142605

[8] Aljewaw, O. B., M. K. A. Karim, N. Effendy, H. M. Kamari, M. H. M. Zaid, N. M. Noor, A. A. Salim et al. "Physical, optical and thermoluminescence properties of lithium aluminum borate glass co-doped with Dy_2O_3." *Radiation Physics and Chemistry* 209 (2023): 111004. https://doi.org/10.1016/j.radphyschem.2023.111004

[9] Aljewaw, Osama Bagi, Muhammad Khalis Abdul Karim, Halimah Mohamed Kamari, Mohd Hafiz Mohd Zaid, Noramaliza Mohd Noor, Iza Nurzawani Che Isa, and Mohammad Hasan Abu Mhareb. "Impact of Dy_2O_3 substitution on the physical, structural and optical properties of lithium-aluminium-borate glass system." *Applied Sciences* 10, no. 22 (2020): 8183. https://doi.org/10.3390/app10228183

[10] Efenji, G. I., Iskandar Shahrim Mustafa, O. O. Ogunleye, Thair Hussein Khazaalah, Nabasu Seth Ezra, Hayder Salah Naeem, Hanisha Mohd Shariff, Munirah Jamil, and Muhammad Fadhirul Izwan Abdul Malik. "Description and dosimetric features of lithium borate glass doped with transition metals for thermoluminesce, a re-evaluation." *Physica Scripta* 98, no. 5 (2023): 052001. https://doi.org/10.1088/1402-4896/acc23c

[11] Efenji, G. I., S. M. Iskandar, N. N. Yusof, J. A. Rabba, O. I. Mustapha, I. M. Fadhirul, S. A. Umar et al. "Structural Properties of Thermoluminescence Dosimeter Materials, Preparation, Application, and Adaptability: A Systematic Review." *Journal of Applied Sciences and Environmental Management* 28, no. 4 (2024): 1129-1150. https://doi.org/10.4314/jasem.v28i4.13

[12] Alege, G. O., B. H. Ojo, G. I. Ifenji, J. B. Kachi, F. O. Tawose, E. Glen, and E. O. Oladimeji. "Cytogenetic effects of radiation from projector on meristematic cells of Allium cepa (onions) root." *Journal of Applied Sciences and Environmental Management* 26, no. 4 (2022): 737-744. https://doi.org/10.4314/jasem.v26i4.25

[13] Jamil, Munirah, Iskandar Shahrim Mustafa, Naser Mahmoud Ahmed, Shahrul Bariyah Sahul Hamid, Thair Hussien Khazaalah, Efenji Godwin, Nabasu Seth Ezra, and Hayder Naeem Salah. "Poly (ethylene) oxide/erbium oxide as T2 and T1-T2 dual-mode MRI diagnostic nanofibres." *Ceramics International* 49, no. 13 (2023): 22429-22439. https://doi.org/10.1016/j.ceramint.2023.04.072

[14] Balu, L., R. Amaravel, and R. Ezhil Pavai. "Effect of ZnO on physical, structural and mechanical properties of B_2O_3-Na_2O-ZnO glasses." *IOSR Journal of Applied Physics* 8, no. 6 (2016): 140-146.

[15] Khandaker, Mayeen Uddin, Ali Taheri, and David Andrew Bradley. "A systematic review on the silica fibre thermoluminescence dosimeters for medical applications." *Journal of Radioanalytical and Nuclear Chemistry* 333, no. 3 (2024): 1507-1530. https://doi.org/10.1007/s10967-023-09109-7

[16] Efenji, G. I., J. T. Zhimwang, M. M. Gwani, J. M. Uzer, and S. A. Kazeem. "Design and Construction of a Smart-home Automation System (SHAS) using Nodemcu and Google Assistant." *Asian Journal of Research and Reviews in Physics* 5, no. 4 (2021): 1-10. https://doi.org/10.9734/ajr2p/2021/v5i430168

[17] Rabba, J. A., F. O. Uloko, G. I. Efenji, S. O. Eghaghe, H. A. Jaafar, M. Z. M. Jafri, and N. D. Osman. "Assessment of Correlation between Dimensions of Ball Phantom and Distortion Rate of Panoramic Radiography in Dental Cone Beam Computed Tomography." *Journal of Applied Sciences and Environmental Management* 27, no. 11 (2023): 2469-2474. https://doi.org/10.4314/jasem.v27i11.15

[18] Efenji, G. I., E. O. Obi, F. A. Kamgba, and Ituabhor Odesanya. "Gas flaring effects on temperature change in Amai Community area in Niger Delta region of Nigeria." *IOSR Journal of Applied Physics* 6, no. 2 (2014): 40-45. https://doi.org/10.9790/4861-06234045

[19] Khazaalah, Thair Hussein, Iskandar Shahrim Mustafa, M. I. Sayyed, Azhar Abdul Rahman, Mohd Hafiz Mohd Zaid, Rosdiyana Hisam, Muhammad Fadhirul Izwan Abdul Malik, Nabasu Seth Ezra, Hayder Salah Naeem, and Nuridayanti Che Khalib. "Development of novel transparent radiation shielding glasses by BaO doping in waste soda lime silica (SLS) glass." *Sustainability* 14, no. 2 (2022): 937. https://doi.org/10.3390/su14020937

[20] Egeonu, Eugene K., O. D. Osahon, I. Efenji Godwin, and M. Anoruo Chukwuma. "Comparative Assessment of Electrical Properties and pH of Homemade and Industrial Pineapple Juice Samples from Benin City." *International Journal of Applied Science and Mathematical Theory* 3, no. 2 (2017).

[21] Zaman, Haydar Uz. "Fabrication and Analysis of Physico-Mechanical Characteristics of Chemically Treated Bhendi Fiber Reinforced Thermoplastic Composites: Effect of UV Radiation." *Malaysian Journal on Composites Science and Manufacturing* 13, no. 1 (2024): 1-13. https://doi.org/10.37934/mjcsm.13.1.113

[22] Mahmood, M. Masood, M. Basim Kakakhel, M. Wazir-ud-Din, Sikander Hayat, Khalil Ahmad, M. Tariq Siddique, Atif Masood, and Sikander M. Mirza. "Thermoluminescence (TL), kinetic parameters and dosimetric features of Pakistani limestone." *Applied Radiation and Isotopes* 188 (2022): 110357. https://doi.org/10.1016/j.apradiso.2022.110357

[23] Joseph, Tresa A., Vibha Chopra, Marta Michalska-Domanska, and Sanjay J. Dhoble. "A scrutiny of phosphors for TL radiation dosimetry." In *Radiation Dosimetry Phosphors*, pp. 45-70. Woodhead Publishing, 2022. https://doi.org/10.1016/B978-0-323-85471-9.00014-2

[24] Saidu, A., H. Wagiran, M. A. Saeed, and Y. S. M. Alajerami. "Structural properties of zinc lithium borate glass." *Optics and Spectroscopy* 117 (2014): 396-400. https://doi.org/10.1134/S0030400X14090239

[25] Saidu, A., H. Wagiran, M. A. Saeed, and Y. S. M. Alajerami. "Thermoluminescence characteristics of zinc lithium borate glass activated with Cu+ (ZnO-Li_2O-B_2O_3+) for radiation dosimetry." *Journal of Radioanalytical and Nuclear Chemistry* 304, no. 2 (2015): 627-633. https://doi.org/10.1007/s10967-014-3846-y

[26] Ullah, Bait, Muhammad Basim Kakakhel, Shakeel Ur Rehman, Muhammad Tariq Siddique, Khalil Ahmad, Muhammad Masood Mahmood, and Iftikhar Anjum. "Thermoluminescence dosimetric characteristics and glow curve analysis of Eocene rock salt, the gray halite, mined from Bahadur Khel site, Pakistan." *Journal of Luminescence* 271 (2024): 120622. https://doi.org/10.1016/j.jlumin.2024.120622

[27] Wazir-ud-Din, Mirza, Dirk Poelman, Johan De Grave, Dimitri Vandenberghe, Muhammad Basim Kakakhel, Sikander Hayat, and Nasrin Karimi Moayed. "Thermoluminescence dosimetric and kinetic characterization of Pakistani fluorite after β irradiation." *Nuclear Instruments and Methods in Physics Research Section B: Beam Interactions with Materials and Atoms* 540 (2023): 246-258. https://doi.org/10.1016/j.nimb.2023.04.031

[28] Nur, N., Z. Yeğingil, M. Topaksu, K. Kurt, T. Doğan, N. Sarıgül, M. Yüksel et al. "Study of thermoluminescence response of purple to violet amethyst quartz from Balikesir, Turkey." *Nuclear Instruments and Methods in Physics Research Section B: Beam Interactions with Materials and Atoms* 358 (2015): 6-15. https://doi.org/10.1016/j.nimb.2015.05.011

[29] McKeever, S. W. S., S. Sholom, and J. R. Chandler. "Developments in the use of thermoluminescence and optically stimulated luminescence from mobile phones in emergency dosimetry." *Radiation Protection Dosimetry* 192, no. 2 (2020): 205-235. https://doi.org/10.1093/rpd/ncaa208

[30] Thabit, Hammam Abdurabu, Norlaili A. Kabir, Abdulmajeed Muidh Al Mutairi, Abdullah Bafaqeer, Shoroog Alraddadi, Nuru-Deen Jaji, M. I. Sayyed, and Salem Mgammal Al-Ameri. "Investigation of the thermoluminescence dosimeter characteristics of multilayer ZnO (300 nm)/Ag (50 nm)/ZnO (x) thin films for photonic dosimetry applications." *Optical Materials* 137 (2023): 113548. https://doi.org/10.1016/j.optmat.2023.113548

[31] Muhammad, N. A., Muhammad Khalis Abdul Karim, Hasyma Abu Hassan, Mazliana Ahmad Kamarudin, Jeannie Hsiu Ding Wong, and Mohammad Johari Ibahim. "Estimation of effective dose and organ cancer risk from paediatric computed tomography thorax-abdomen-Pelvis examinations." *Radiation Physics and Chemistry* 165 (2019): 108438. https://doi.org/10.1016/j.radphyschem.2019.108438

[32] Pal, Manisha, Baishakhi Roy, and Mrinal Pal. "Structural Characterization of Borate Glasses Containing Zinc and Manganese Oxides." *Journal of Modern Physics* 2, no. 9 (2011): 1062-1066. https://doi.org/10.4236/jmp.2011.29129

[33] Patwari, D. Rajeshree, and B. Eraiah. "Luminescence properties of erbium doped sodium barium borate glass with silver nanoparticles." In *IOP Conference Series: Materials Science and Engineering*, vol. 310, no. 1, p. 012056. IOP Publishing, 2018. https://doi.org/10.1088/1757-899X/310/1/012056

[34] Muhammad, N. A., Muhammad Khalis Abdul Karim, Hasyma Abu Hassan, Mazliana Ahmad Kamarudin, Jeannie Hsiu Ding Wong, and Mohammad Johari Ibahim. "Estimation of effective dose and organ cancer risk from paediatric computed tomography thorax-abdomen-Pelvis examinations." *Radiation Physics and Chemistry* 165 (2019): 108438. https://doi.org/10.1016/j.radphyschem.2019.108438

[35] Atlıhan, Mehmet Altay. "Thermoluminescence properties of two natural colorful fluorite samples of Anatolian origin for dosimetric applications." *Nuclear Instruments and Methods in Physics Research Section B: Beam Interactions with Materials and Atoms* 467 (2020): 33-39. https://doi.org/10.1016/j.nimb.2020.02.002

[36] Naseer, K. A., K. Marimuthu, M. S. Al-Buriahi, Amani Alalawi, and H. O. Tekin. "Influence of Bi2O3 concentration on barium-telluro-borate glasses: physical, structural and radiation-shielding properties." *Ceramics International* 47, no. 1 (2021): 329-340. https://doi.org/10.1016/j.ceramint.2020.08.138

[37] Saidu, A., H. Wagiran, M. A. Saeed, H. K. Obayes, A. Bala, and F. Usman. "Thermoluminescence response of rare earth activated zinc lithium borate glass." *Radiation Physics and Chemistry* 144 (2018): 413-418. https://doi.org/10.1016/j.radphyschem.2017.10.004

[38] Yılmaz, Demet, and Tuba Akkuş. "An experimental work on radiation scattering features of some thermoluminescent dosimetry materials." *Radiation Physics and Chemistry* 216 (2024): 111456. https://doi.org/10.1016/j.radphyschem.2023.111456